JTTEE5 10:470-479
© ASM International

Peer Reviewed

The Effect of Post-Treatment of a High-Velocity Oxy-Fuel Ni-Cr-Mo-Si-B Coating Part I: Microstructure/Corrosion Behavior Relationships

S. Shrestha, A. Neville, and T. Hodgkiess

(Submitted 28 July 2000)

The microstructure and aqueous corrosion characteristics of a Ni-Cr-Mo-Si-B high-velocity oxy-fuel (HVOF) coating have been assessed. It has been shown that postprocessing by vacuum fusion has a significant effect on the coating microstructure by increasing the type and concentration of hard phase particles. The principal hard phases in the as-sprayed condition and vacuum-sealed condition are chromium carbides, whereas molybdenum-containing boride phases are also present after vacuum fusion. Vacuum-fusion post-treatment eliminates splat boundaries, which can act as sites, where preferential corrosion can occur and, hence, the dominant corrosion mechanisms change. In as-sprayed and vacuum-sealed coatings, localized attack at splat particle boundaries and crevice corrosion dominate, whereas in vacuum-fused coating, the principal mechanism of corrosion is "micropitting" as a result of the hard phase loss.

Keywords cermet, corrosion, hard phase, HVOF spraying, vacuum fusion, vacuum sealing

1. Introduction

Surface engineering by application of thermal spray coatings (TSCs) is increasingly being used for critical industrial components where even the highest-grade metallic materials can show limitations in performance. Much of the initial development of TSCs was focused toward improving the wear performance of surfaces in dry and lubricated conditions. This was driven to a large extent by the applications in the aerospace industry, where the first thermal spray coatings were employed.[1] The potential for utilizing TSCs in applications outside the aerospace sector has been realized over the last decade and TSCs are being used or considered seriously for components in a diverse range of industries including oil recovery and refining,[2,3] paper manufacture,[4] and automotive industry.[5,6]

Many potential applications of TSCs involve offering protection to components, which will be exposed to wear in an aqueous system. In such circumstances, the electrochemical corrosion characteristics of the coating must be considered. This is important for two reasons: first, it is of importance where the component is required to remain immersed in a static electrolytic solution for periods during plant shutdown; and, second, it is known from studies on metallic materials[7,8] that corrosion can play a very important role in the degradation of materials in environments where wear occurs in an aqueous environment.

S. Shrestha and **T. Hodgkiess,** Department of Mechanical Engineering, University of Glasgow, Glasgow G12 8QQ, Scotland, United Kingdom; and **A. Neville,** Department of Mechanical and Chemical Engineering, Heriot-Watt University, Edinburgh, EH14 4AS, Scotland, United Kingdom. Contact e-mail: skshrestha@twi.co.uk.

It has been the case during development of TSCs that the key issue relating to their corrosion behavior is the interconnected porosity and the ability of the liquid phase to penetrate into the coating/substrate interface.[9] However, thermal spray cermet coatings comprising ceramic hard phases embedded in a metallic matrix represent extremely complex materials from an electrochemical point of view, and, even in the absence of interconnected porosity, there is scope for complex corrosion mechanisms to occur, which will lead to deterioration of the coating. Indeed, several studies by the authors have demonstrated on a variety of TSCs that the inherent corrosion resistance of the coating is a factor that must be considered when coatings are to be employed in aqueous systems.[10,11]

In this paper, the corrosion characteristics of a Ni-Cr-Mo-Si-B coating applied by the high-velocity oxy-fuel (HVOF) process are assessed in the as-sprayed condition, after polymer impregnation sealing and after vacuum furnace fusion. The paper focuses on the effect of corrosion behavior in terms of electrochemical measurements and observed mechanisms in relation to the coating microstructure. In part II, the coating resistance to degradation in erosion-corrosion conditions is scrutinized.

2. Experimental

2.1 Material and Specimen Preparation

One generic type of coating has been studied in this work: a Ni-Cr-Mo-Si-B cermet coating applied by the HVOF process utilizing Tafa's JP-5000 high-pressure HVOF system with liquid kerosene fuel burning in oxygen. The specified composition of the coating is 67.5% Ni 16% Cr 3.5% Si 3.5% B3% Mo 3% Cu 4% Fe 0.8% C (Tafa's powder 1275H). The powder and coating microstructural characteristics and the static corrosion behavior of the coating were investigated. The coating was studied

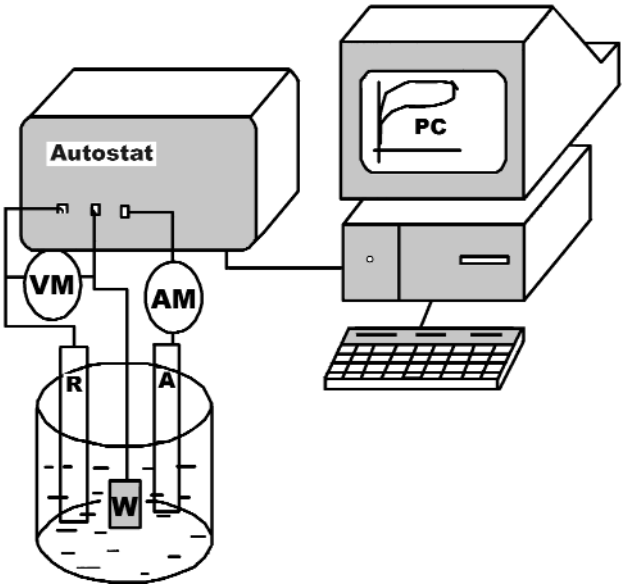

Fig. 1 Schematic diagram of a three-electrode electrochemical cell: R—reference electrode, W—working electrode, and A—auxiliary electrode

in the as-sprayed condition, after sealing using a polymeric sealant (vacuum-sealed) and also after a post-treatment by vacuum furnace fusion (vacuum-fused).

Vacuum furnace fusion was conducted at a temperature between the liquidus and solidus states (1050 to 1150 °C). This process was carried out commercially. Also, the coatings were commercially applied to a BS970 EN8 carbon-steel plate. Specimens, 1 × 1 cm for corrosion and microstructural examination were cut from the as-received plates. Electrical connecting wires were soldered to the back (steel) face of the samples prior to encapsulation in a nonconducting resin. The specimens were mounted in plane (*i.e.*, with the coated face exposed). Finally, the samples were ground on abrasive papers and polished to a 1 μm diamond finish. Prior to any corrosion testing, the coatings were examined in plane and in cross section, which enabled the interface between the coating and the substrate to be examined.

2.2 Corrosion Tests

Static corrosion experiments were carried out by immersion of the specimens in a seawater solution made up using a proprietary product, "Instant Ocean" (manufactured by Aquarium Systems, Mentor, OH), that contains all the major ionic constituents of seawater, dissolved in distilled water to yield a salinity of 35,000 ppm. The specimen/resin interfaces of the encapsulated specimens were painted with a sealing lacquer, "Lacomit" (manufactured by Bio-rad, Hemel Hempstead, United Kingdom) to prevent interference in the electrochemical measurements from the substrate material. After 1 h of immersion in the seawater at either ambient temperature (18 °C) or 50 °C, the specimens were subjected to standard DC anodic polarization potentiodynamic scans using a standard three-electrode electrochemical cell, as shown in Fig. 1. The potential scan rate was 15 mV/min. All potentials were measured using the saturated calomel reference electrode (SCE), and the auxiliary electrode used was platinum. Additionally, free-corrosion experiments were conducted in which specimens were exposed to the seawater at 18 °C for periods of up to 1 month and subsequently examined without any electrochemical testing.

2.3 Microstructural Characterization

Microstructural examination of as-received coatings (in plane and cross section) and specimens after corrosion tests was performed using light optical microscopy and scanning electron microscopy (SEM, Cambridge Stereo Scan-360, Cambridge Instruments, Cambridge, United Kingdom). Quantification of the porosity on a 100 × 100 μm area and the hard phase content from a 25 × 25 μm area was done using Aequitas Image Analysis software (Dynamic Data Links Ltd.). Energy dispersive x-ray (EDX) analysis was undertaken using the attachment on the SEM, and the facility also provided quantitative (atomic number, absorption, and fluorescence) correction procedures for spot analyses. Spot analyses were undertaken on hard phase particles or matrix areas of sizes of 3 μm or greater. X-ray diffraction (XRD) measurements were taken on powder samples and on the surfaces of the coated plates using the Philips PW 1050/35 x-ray diffractometer (Philips Electronic Instruments Corp., Mahwah, NJ).

Microhardness measurements were made using Buehler Micromet®-II according to ASTM standard E-384-73. An assessment of the coating density was made by accurately weighing the samples before and after spraying and then calculating from the volume of the coating deposited. This procedure was undertaken on ten samples to yield an average value of the coating density.

Results

3.1 Characterization of Powders

Figure 2(a) shows the spherical powder particles of diameter 3 to 40 μm, and Fig. 2(b) shows a higher magnification split SEM image of the powder particle in the cross section. The distribution of hard phases in the powder particles is clear. Analysis of the feedstock powder by XRD showed that there are two primary constituents of the hard phase: $Cr_{23}C_6$ and Cr_3NiB_6 (Fig. 3a). The matrix is a solid solution of NiCrFe. Analysis of individual powder particles by EDX showed that, although the Fe, Si, and Cu contents are relatively consistent, there are variations in the Ni, Cr, and Mo contents such that particles enriched in Ni were denuded in Cr and Mo. The analyses taken on seven particles are shown in Table 1.

3.2 Characterization of Coatings

The characteristics of the coatings are detailed in Table 2. It can be seen that the as-sprayed and vacuum-sealed coatings display very similar characteristics, but the vacuum-fused coating resulted in a lower porosity, higher hardness, higher hard phase content, and higher density. The as-received surface of the coating after vacuum fusion is smoother (lower microroughness, R_a) than the nonfused (as-sprayed and vacuum-sealed) coatings, giving an indication of the consolidation effect of the post-treatment.

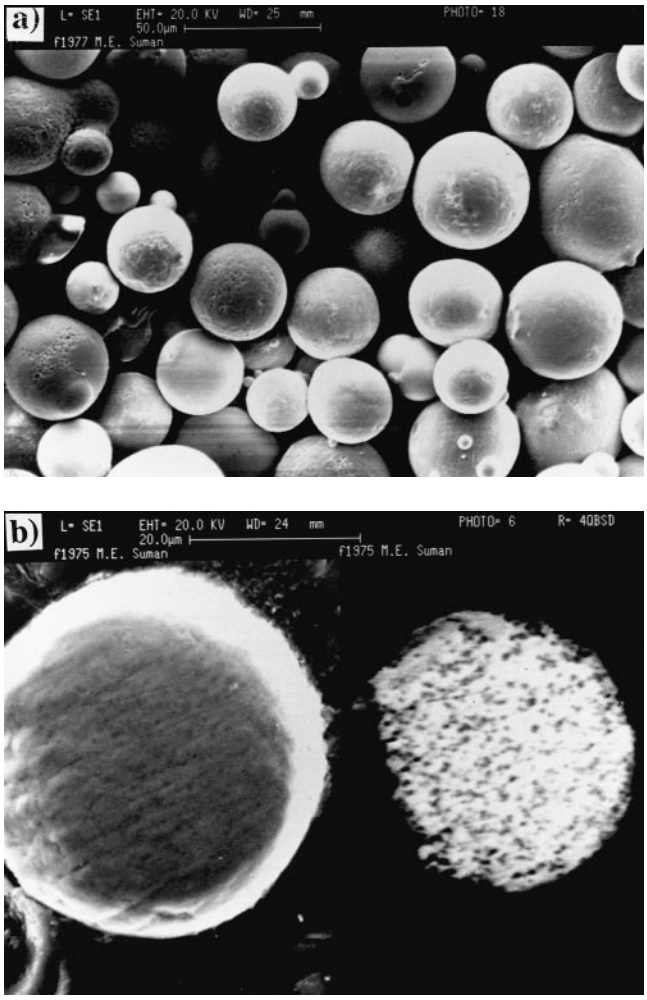

Fig. 2 (**a**) Particles of the Ni-Cr-Mo-Si-B coating powder. (**b**) Secondary (left) and backscattered (right) SEM images of the polished powder particle

Table 1 EDX analyses on individual powder particles

Element (wt.%)	1	2	3	4	5	6	7
Fe	2.5	2.9	2.5	3.2	2.9	2.9	2.7
Ni	62.8	62.7	61.6	74.2	67.0	59.1	65.2
Cr	16.1	17.4	17.3	11.0	13.0	20.0	12.4
Si	3.8	3.6	3.6	4.4	4.0	3.6	4.4
Mo	5.8	6.1	6.7	2.9	2.7	8.1	3.5
Cu	1.8	1.9	1.7	2.0	1.8	1.8	1.8

3.3 Microstructural Examination of the As-Polished Coating

As-Sprayed/Vacuum-Sealed Coating. Both as-sprayed and vacuum-sealed coatings show similar microstructures and, hence, hereafter will be referred to as-sprayed/sealed, implying both types of coatings. Examination of the sprayed/sealed coating cross section revealed low coating porosity and low interfacial porosity, as shown on the backscattered SEM image of the cross section (Fig. 4). The individual splat lamellae can be seen overlapping one another. At higher magnification, the SEM

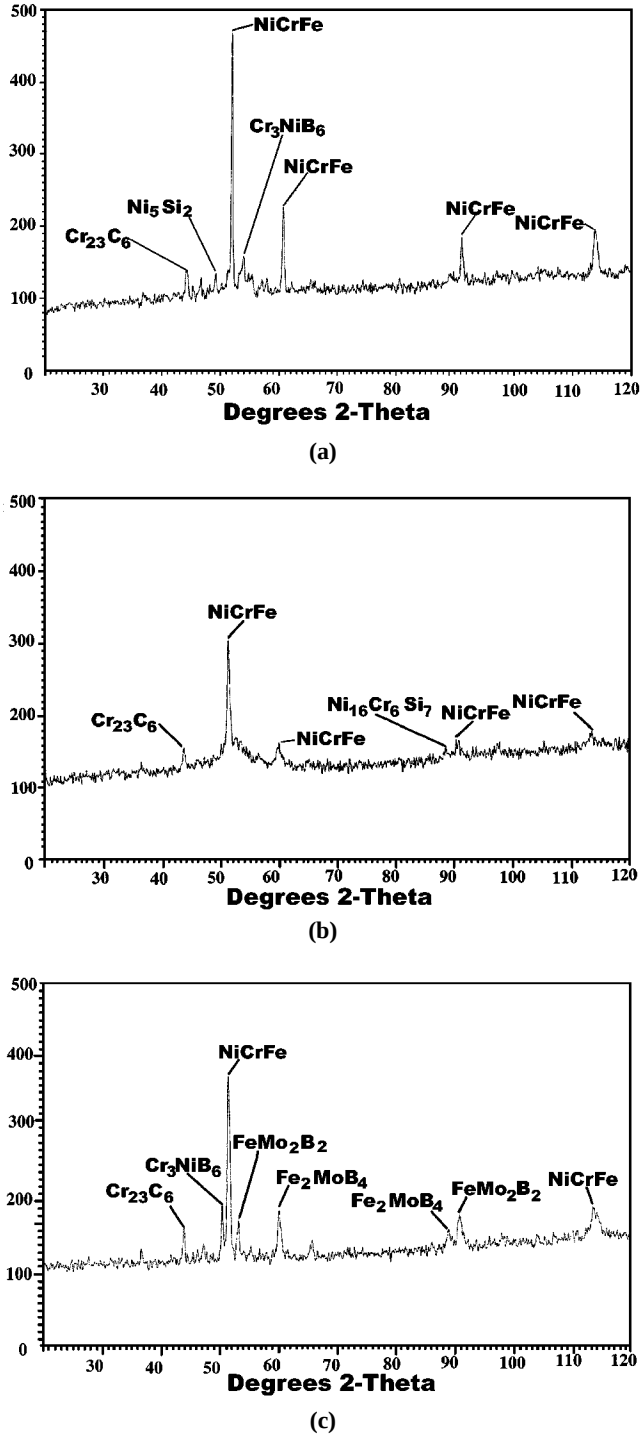

Fig. 3 (**a**) XRD trace of the powder. (**b**) XRD trace of the as-sprayed coating. (**c**) XRD trace of vacuum-fused coating

image of the polished plane surface showed a clear abundance of black (low atomic number) globular hard phase particles of sizes varying from 0.2 to 3 μm (Fig. 5). Both spot and bulk analyses of the hard phase particles "2" and the binding matrix "1" were taken using EDX, and the analyses are listed in Table. 3. Notwithstanding the small size of the hard phase particles, it

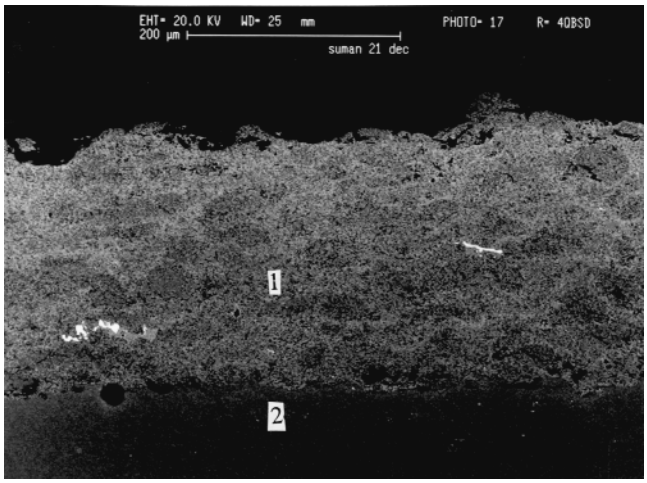

Fig. 4 Backscattered SEM image of the as-sprayed coating cross section (1—coating, and 2—substrate)

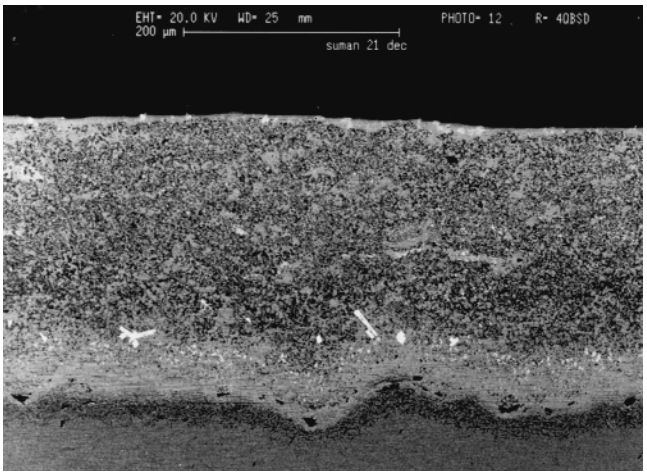

Fig. 6 Backscattered SEM image of the vacuum-fused coating in cross section

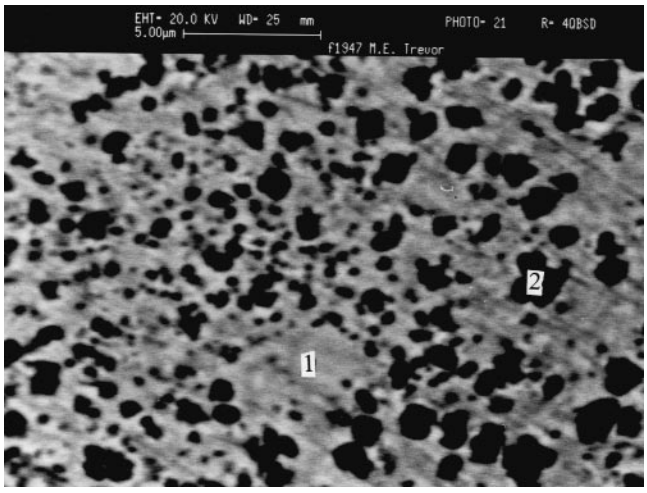

Fig. 5 Backscattered SEM image of the as-sprayed coating showing the distribution of hard phase particles (dark)

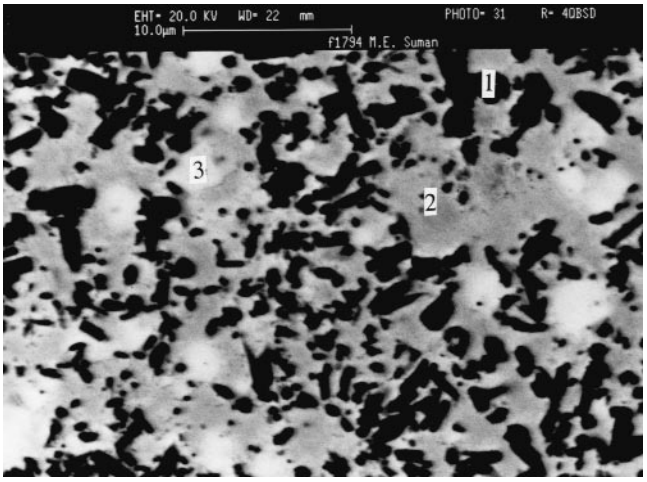

Fig. 7 Backscattered SEM micrograph of the vacuum-fused coating showing the higher density of dark hard phase particles "1" than in the as-sprayed coating, matrix "2," and distribution of Mo-rich blocky white particles "3"

Table 2 Characterization of the coating

Coating type	Coating porosity (%)	Hard phase 2 distribution (% area)	Vickers Hardness ($HV_{0.5}$)	Thickness (μm)	R_a (μm)	Density (g/cm^3)
Sprayed	1.5–2.73	14 ± 5	612–692	240 ± 25	8.7	6.60
Sealed	1.7–2.41	14 ± 5	546–716	240 ± 25	8.5	6.65
Fused	0.23–0.33	29 ± 3	816–876	260 ± 10	3.5	8.30

was shown that they were rich in Cr and Mo. X-ray diffraction analysis (Fig. 3b) confirmed the principal hard phase particles within the metal matrix to be the carbide compound ($Cr_{23}C_6$), and no Mo-containing crystalline phase was identified. The metal matrix was nickel rich, identified by XRD to be NiCrFe.

Vacuum-Fused Coating. The vacuum furnace fusion altered the coating microstructure significantly, which was clearly discernible in both cross-sectional (Fig. 6) and planar views. The more dense abundance of larger dark acicular hard phases than in the as-sprayed or vacuum-sealed coatings was quite clear under the backscattered image of the coating (Fig. 7). In addition to these dark hard phases, an abundance of blocky white (higher atomic numbered) hard phase particles were visible, which were found to be rich in molybdenum. The XRD results (Fig. 3c)

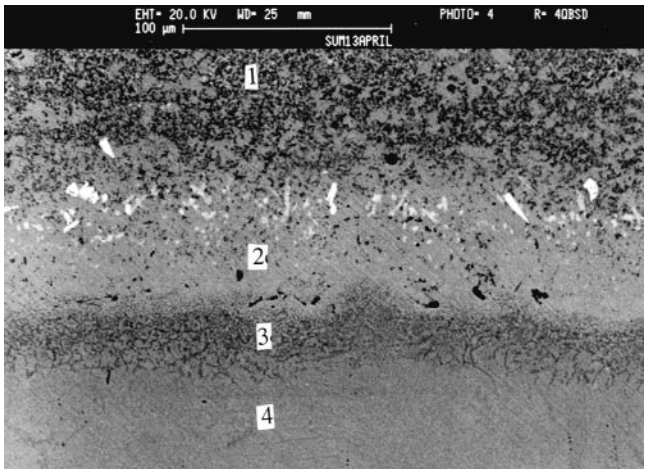

Fig. 8 Diffusion zone at the interface of the vacuum-fused coating and the steel substrate (1—main coating, 2—interdiffusion layer in coating, 3—diffusion zone in substrate, and 4—steel substrate)

Table 3 Measured composition by EDX on the hard phase, matrix, and area of the as-sprayed coating shown in Fig. 5

Element	Matrix (wt.%)	Globular hard phase (wt.%)	100 × 100 μm area of coating
Fe	3.0–3.3	1.9–2.3	2.7–3.0
Ni	77.7–81.9	25.1–32.5	62.7–67.7
Cr	9.8–14.3	38.8–42.2	16.9–17.7
Si	4.8–5.2	1.2–1.6	3.6–4.0
Cu	1.6–2.3	0.5	1.6–2.0
Mo	2.2–4.1	17.5–19.2	5.9–6.7

Table 4 Chemical composition of the constituents of vacuum-fused coating determined by EDX on the cross section shown in Fig. 7 and 8

Elements	Matrix	Dark acicular hard phase	Blocky white hard phase	Zone 1 bulk coating	Zone 2 mixing zone
Fe	2.6–5.4	0.8–2.2	1.0–1.3	3.0–3.4	12.3–13.4
Ni	78–84.9	18–34	37.7–39.2	62.9–64	71.5–73.8
Cr	4.9–6.8	48–60.1	27.2–32.8	21.8–22.8	7.96–8.02
Si	4.8–5.6	0.8–2.8	6.2–6.5	3.8–4.0	3.5–3.8
Cu	2.0–3.1	0.2–0.3	0.2–0.4	1.2–1.3	1.0–1.2
Mo	0.1–1.2	9.0–12.9	37.3–62	7.8–8.1	1.9–2.0

showed the hard phase particles to be carbides ($Cr_{23}C_6$) and borides (Cr_3NiB_6, $FeMo_2B_2$, and Fe_2MoB_4), which were not present in the as-sprayed coating. The cross-sectional view (Fig. 8) showed that significant interfacial diffusion at the coating-substrate interface had occurred, and this resulted in the removal of the sharp coating/metal interface, which was visible in the as-sprayed or vacuum-sealed coatings and a reduction in interfacial porosity. The coalescing of splat particles due to the high-temperature vacuum-fusion process also resulted in removal of intersplat boundaries in the main coating (zone 1), as shown in Fig. 8. Table 4 details the EDX results at spot positions across the interface of the coating after the fusion process. This shows that there is an interdiffusion layer (zone 2), where coating and substrate constituents have been mixed to a large extent.

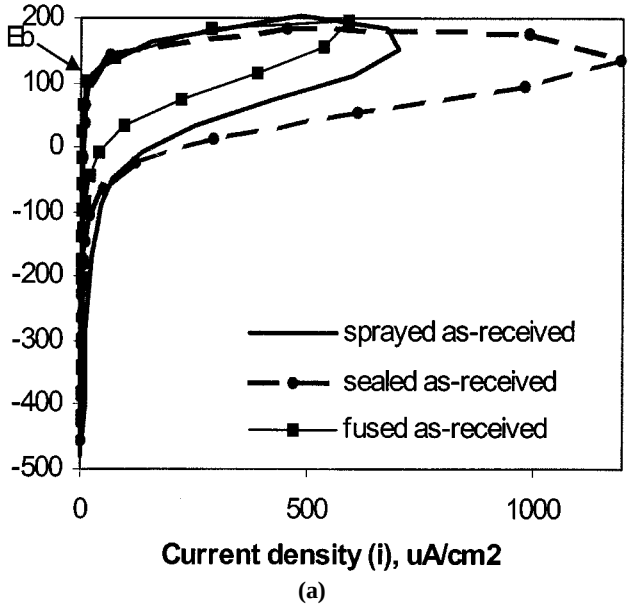

(a)

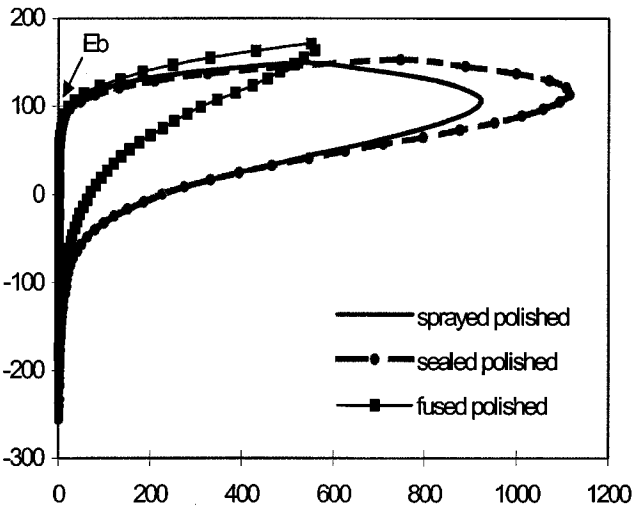

(b)

Fig. 9 (**a**) Anodic polarization of the as-sprayed, vacuum-sealed, and vacuum-fused coating in static seawater at 18 °C. The surfaces were tested as-received. (**b**) Anodic polarization on polished surfaces of the as-sprayed, vacuum-sealed, and vacuum-fused coating in static seawater at 18 °C

3.4 Electrochemical Corrosion Tests

Accelerated anodic polarization tests were conducted on each of the samples in the as-received condition and then after polishing to a 1 μm diamond finish. Figure 9(a) shows the typical anodic polarization plots on the three coatings (as-sprayed, vacuum-sealed, and vacuum-fused) in the as-received condition at 18 °C, and Fig. 9(b) shows the response after polishing at the same temperature. It is clear that there is no difference between the response of the three coatings in a saline solution at 18 °C. All coatings exhibit very low currents on shifting the potential

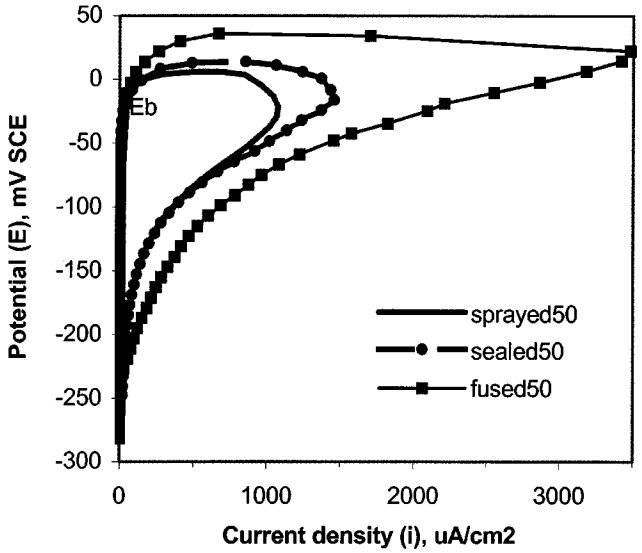

Fig. 10 Anodic polarization on polished surfaces of the as-sprayed, vacuum-sealed, and vacuum-fused coating in static seawater at 50 °C

Table 5 Parameters from anodic polarization of HVOF coating in static saline solution (35,000 ppm) at 18 °C

	E_b (mV, SCE) As-sprayed	E_b (mV, SCE) As-polished	i_{max} (μA/cm^2)
As-sprayed	95–110	85–105	705–920
Vacuum-sealed	100–105	80–90	1115–1195
Vacuum-fused	90–105	90	560–693

from the free corrosion potential E_{corr} for a potential range up to +100 mV (SCE). At this point (denoted the breakdown potential, E_b), a rapid rise in current is observed and this indicates that corrosion has initiated. The scan reverses (*i.e.*, the potential is shifted to more negative values) when a current density of 500 μA/cm^2 is attained and the potential moves toward the free corrosion potential. The maximum current reached on reversal of the potential scan is indicative of the extent to which corrosion can propagate once corrosion has initiated. Table 5 gives details of the parameters, shown in Fig. 9(a), from the anodic polarization curves. A range of values is given to reflect the reproducibility obtained from the three replicate experiments, which were carried out in each case.

It is apparent from Table 5 that, although there is no difference in E_b, and hence the ability for corrosion to initiate, it would appear that the vacuum-fused coating is less susceptible to corrosion propagation, as shown by the lower current density i_{max} attained during anodic polarization.

It is well known that temperature plays an important role in the initiation and propagation of corrosion on passive materials such as stainless steels.[12] In this study, the experiments were also undertaken at 50 °C and the effect on the anodic polarization curve was assessed. In a comparable manner to passive alloys, it was shown that the resistance to the onset of corrosion was lessened as the temperature was increased. Figure 10 shows how E_b was reduced at the higher temperature, and, interestingly, the three coatings, as at 18 °C, showed comparable breakdown

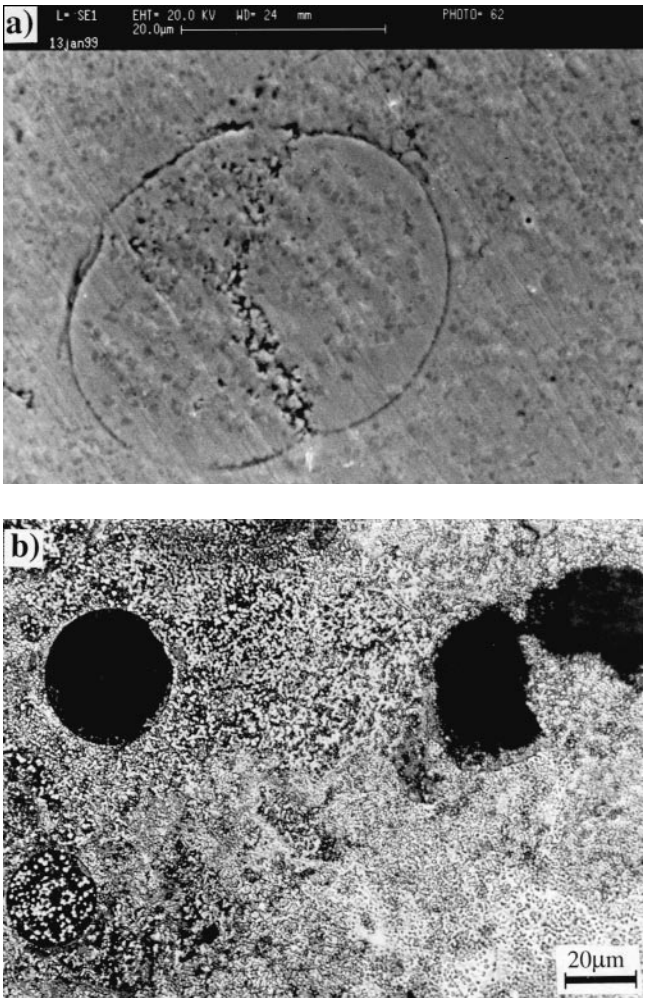

Fig. 11 (**a**) Attack initiation at the splat boundaries on the as-sprayed coating after anodic polarization in static seawater at 18 °C. (**b**) Macropitting as a result of splat removal and the corrosion of matrix leaving the hard phases unsupported on the as-sprayed coating after 1 month exposure under free corrosion potential E_{corr} in static seawater at 18 °C

characteristics. However, in contrast with the results trend at 18 °C, the fused coating supported much higher maximum current density (3500 μA/cm^2) than the as-sprayed (1080 μA/cm^2) and vacuum-sealed (1460 μA/cm^2) coatings. This may signal that the fused coating is more susceptible to corrosion propagation at elevated temperature than as-sprayed and vacuum-sealed coatings, and this is also supported by a slightly larger pit depth measurement (7 μm on the vacuum-fused coating compared to 5 μm on the as-sprayed and vacuum-sealed coatings, Table 6). However, all the coatings displayed similar E_b values at 50 °C, which indicates similar resistance to the onset of corrosion. Further detailed investigations are required to obtain a definitive assessment of the influence of temperature on the corrosion behavior of these coatings.

3.5 Free Corrosion Experiments

Specimens were exposed in the naturally corroding condition at 18 °C with examination after 1, 2, and 4 weeks. Microscopic

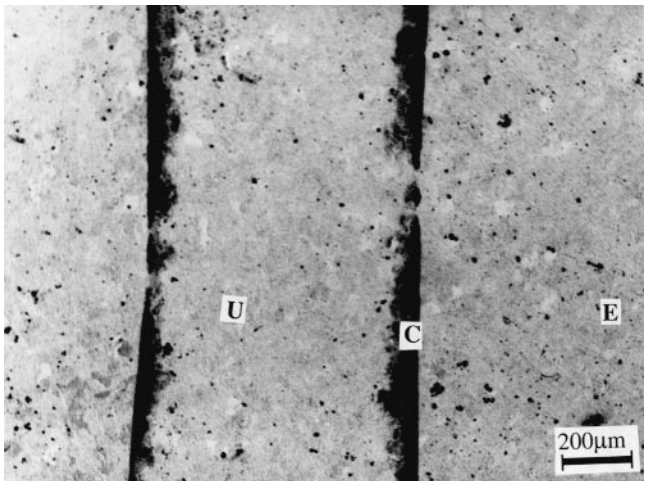

Fig. 12 Crevice corrosion at the Lacomit sealant interface on the as-sprayed coating after anodic polarization at 18 °C (U—under lacomit strip, C—crevice, and E—exposed surface to the electrolyte)

observation after 1 week of immersion showed visible corrosion product on the exposed surface of the as-sprayed and vacuum-sealed coatings, but the vacuum-fused coating exhibited no significant change of its exposed surface. After 2 weeks of immersion, attack was revealed on the vacuum-fused coating. The specimen observed after a 1 month period showed heavy corrosion product on both as-sprayed (Fig. 11b) and vacuum-sealed coatings, but the vacuum-fused coating (Fig. 13b) exhibited relatively much less corrosion product.

3.6 Attack Mechanisms

Analysis of the electrochemical measurements (anodic polarization) by consideration of the parameter E_b, which is most commonly used to indicate resistance to the onset of corrosion, does not show any difference in the relative performance of the as-sprayed, vacuum-sealed, and vacuum-fused coatings. However, close examination of the extent of corrosion attack and the attack mechanisms shows that there is a difference, which accounts for the variations in i_{max} depending on the post-treatment of the coating and/or the temperature.

As stated earlier in the paper, after fusion of the coating, no splat boundaries were detected, and this has been shown in this study to have implications for the corrosion resistance of the coating. As detailed in Table 6, especially at 50 °C, there is severe attack at the splat boundary, possibly due to a microcrevice corrosion mechanism, and this can lead to removal of entire splats to form "macropits." Figure 11(a) shows the initiation stage of this attack on the as-sprayed coating after anodic polarization at 18 °C, which also shows localized removal of the hard phase particles forming micropits, and Fig. 11(b) shows the "macropitting" as a result of splat removal after 1 month of free exposure at free corrosion potential E_{corr} of the as-sprayed coating specimen surface.

In addition to the localized attack at the splat boundaries, another localized attack mechanism observed was crevice attack, which occurred at the lacomit sealant (Fig. 12). At the crevice regions "C" (dark lines in Fig. 12), deep attack was visible after anodic polarization.

In relation to the vacuum-fused coating, there were no visible splat boundaries and, hence, no corrosion initiation associated with individual splat regions occurred. In addition, there was visibly less severe crevice corrosion observed on the vacuum-fused coating compared with the sprayed/sealed coating. On the vacuum-fused coating, it was evident that the most dominant mechanism of corrosion was in the form of very localized "micropitting," which was clearly associated with the individual hard phase particles and their removal once corrosion of the surrounding material had occurred and that the increase in temperature accentuated the extent of attack, as shown clearly in Fig. 13(a). One month of exposure of the vacuum-fused coating at free corrosion potential E_{corr} and ambient temperature (Fig. 13b) revealed both corrosion of the matrix and preferential severe attack at the hard phase/matrix interface, which resulted in micropitting. Localized removal of the hard phase particles to form micropits was observed also on the as-sprayed coating, as shown in Fig. 11(a).

4. Discussion

Thermal spraying is becoming widely used in aqueous erosion-corrosion environments, and, because of this, there is impetus to improve the corrosion resistance of the coatings, which were typically developed for mechanical wear resistance. In the early development, the principal concern regarding the corrosion behavior of TSCs was considered to be their ability to provide a barrier between the corrosive fluid and the underlying substrate, which is often a low-grade material with poor corrosion resistance. As a result, techniques were developed to post-treat the coating surface as a means of reducing, or even eliminating, interconnected porosity such as polymer impregnation[13,14] and laser treatment.[15,16] As reported by Neville and Hodgkiess[10] on WC-CoCr systems, in the current HVOF coatings, the level of interconnected porosity is very low and, therefore, corrosion by penetration of the coating is not the main concern.[17] Tobe in 1998[18] reported the ineffectiveness of polymer sealant for reducing corrosion attack.

In the work described in the present paper, Ni-Cr-Mo-Si-B self-fluxing coating applied by the HVOF process was examined in the as-sprayed, vacuum-sealed, and vacuum-fused conditions. The aspect of the coating's corrosion behavior under scrutiny was its inherent corrosion resistance, which due to the network of carbides and matrix has the potential to be very complex. In agreement with other workers,[13] it has been shown that application of polymer sealant under vacuum has no beneficial or detrimental effect on the corrosion behavior of the coating. All the coatings possessed very low porosity (estimated to be lower than 3%). Fusion of a thermal-sprayed coating is normally performed when spraying is done by an oxyacetylene process, where the residual porosity is high and there is a genuine need to seal and consolidate the coating. Fusion of HVOF coatings is less common due to their generally high quality. However, in this work, the modification of the microstructure of the coating by the fusion process has been shown to affect the microstructure, microchemical composition, and density and also some aspects of the corrosion behavior and mechanisms.

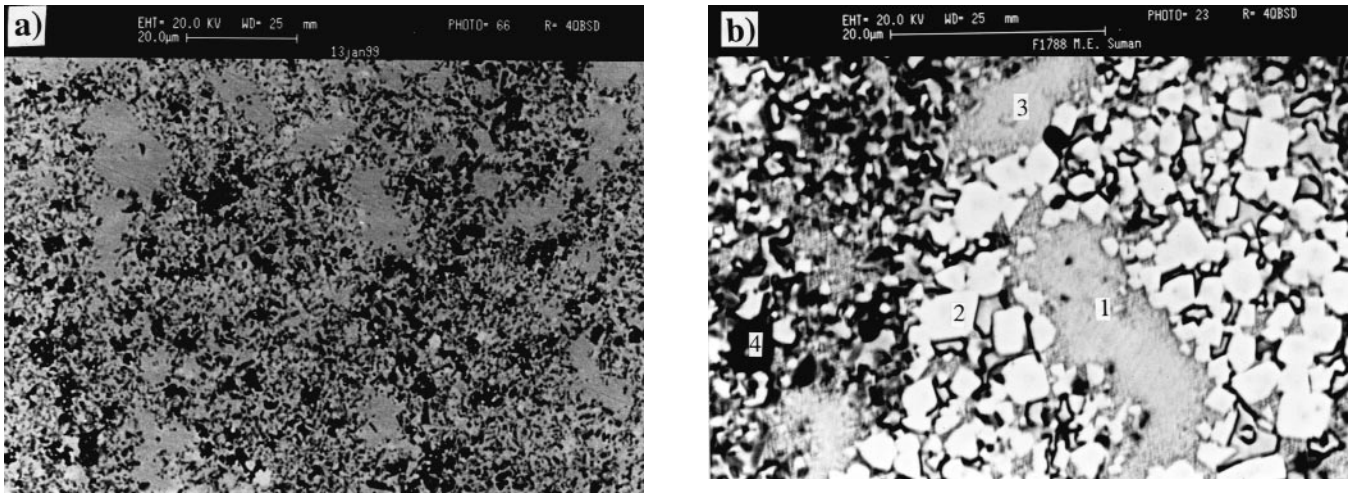

Fig. 13 (**a**) Backscattered SEM micrograph of the vacuum-fused coating showing micropitting on the exposed surface due to removal of individual hard phase particles after anodic polarization at 50 °C. (**b**) Backscattered SEM micrograph of the exposed surface showing matrix "1," "3" corrosion, and severe preferential corrosion attack at the hard phase/matrix interface, leaving the hard phase particles "2" unsupported from the binder matrix, resulting in micropits "4" after 1 month of exposure of the vacuum-fused coating to static seawater under free corrosion potential E_{corr} and 18 °C

Table 6 Corrosion mechanisms on coatings after anodic polarization at two temperatures

	Total crevice length (mm)		Maximum pit depth (μm)		Comments	
	18 °C	50 °C	18 °C	50 °C	18 °C	50 °C
As-sprayed	47–50	9–12	4	5	Corrosion initiation on exposed surface etching effect	Exposed region severe corrosion at splat boundaries
Vacuum-sealed	50–55	35–40	5	5	Similar to above	Similar to above
Vacuum-fused	15–30	12–18	6	7	Less attack than above on exposed regions. No splat boundaries visible. Some micropitting	Etching on free exposed area and micropitting

4.1 Electrochemical Corrosion Behavior

The anodic polarization experiments exhibited passive behavior of all three coatings when they were initially exposed to the seawater. However, it was apparent that complete passivity does not persist for long (1 to 2 weeks) under natural-corrosion exposure to seawater before localized corrosion is initiated.

These coatings, therefore, possess a considerably superior corrosion behavior than carbon steels and, indeed, behave in a rather similar manner to UNS S31603 stainless steel, which also exhibits passive anodic polarization curves but fairly rapid initiation of localized corrosion in seawater. The fairly early onset of corrosion on the coatings is clearly correlated with their complex microstructures, as detailed below.

4.2 Attack Mechanisms

Corrosion on the nonfused coatings, which here include the as-sprayed and vacuum-sealed coating, occurred by a mixture of mechanisms, where corrosion initiated at the microstructural features in a manner that was essentially identical in the anodic polarization and free-corrosion experiments. The schematic diagram in Fig. 14 represents the three key stages involved in the corrosion process, as described below.

- Initial State—As-polished surface appearance before corrosion, microstructural features, and splat boundaries visible.
- Stage I—Attack initiates preferentially at the splat boundaries and these boundaries become prominent. Boundaries are attacked randomly. Initiation of attack at the hard phase/matrix boundaries inside individual splats.
- Stage II—General corrosion of the matrix proceeds inside individual splats with others remaining unattacked. Some hard phase particles become dislodged, resulting in micropitting.
- Stage III—Macropitting occurs when the individual splats are removed. Further attack occurs within the macropit, which works as a local anode cell once the splat has dislodged.

Initiation of corrosion at splat boundaries of thermal-sprayed coatings has been reported previously, where oxide "stringers"

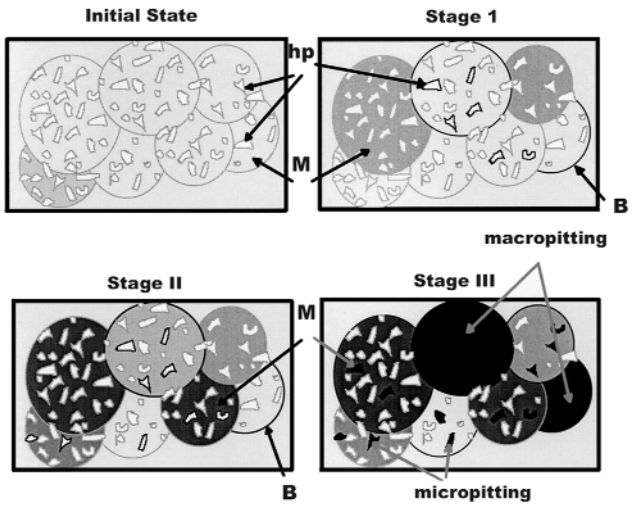

Fig. 14 Schematic representation of corrosion mechanisms occurring on as-sprayed and vacuum-sealed coatings. Initial state—plane surface as-polished; stage I—attack around splat boundary "B" of a splattered particle, corrosion attack initiation around hard phase particles "hp," and matrix "M" starts changing color into light brown; stage II—continuation of corrosion of "M" with conversion into dark brown and around "hp"; and stage III—hard phase particles "hp" and splat particle loss, resulting in both micropitting and macropitting

were found to be responsible for providing a corrosion initiation site.[19] In the corrosion of the coating by the mechanism above, it would appear that, once corrosion is initiated on a particular splat, there is then a microgalvanic action, which prevents subsequent corrosion of the nearest adjoining splats. The surface then corrodes nonuniformly at two levels: *micropitting*, where the hard phase is lost due to corrosion of the supporting matrix; and *macropitting*, where the individual splat is removed. It is possible, in long-term exposures, that this macropitting mechanism might provide paths for the corrosive fluid to penetrate through the coating thickness to cause corrosion and coating adherence problems at the coating/substrate interface, especially with substrate materials of low corrosion resistance such as carbon steel.

4.3 Effect of Postspray Fusion

The differences in electrochemical behavior of the coating with and without fusion were very small. In terms of the resistance of the coating to corrosion initiation, denoted by the breakdown potential, there was no difference at either 18 or 50 °C. More subtle differences were apparent in terms of the maximum currents attained during anodic polarization. Corrosion of the vacuum-fused coating was contrasting in nature mainly due to the fact that there are no visible splat boundaries, which as discussed above act as individual initiation sites for corrosion. Although this did not change the apparent resistance to passivity breakdown, as manifested by the similar E_b values, it could account for the slightly increased times for the initiation of corrosion of fused specimens in the free corrosion tests at 18 °C and the apparent reduced intensity of attack up to 1 month as well as the lower maximum currents in the 18 °C anodic polarization experiments.

In the fused coatings, corrosion initiation was associated primarily with the hard phase particles. There was a higher density of hard phase particles after fusion and their interfaces with the matrix provided sites for corrosion to initiate. A change in the corrosion behavior after fusion is not unexpected given the absence of splat boundaries and also the fact that fusion promotes formation of C- and B-rich phases. These primarily tie up the key species, which confer corrosion resistance (Cr and Mo) and, as clearly demonstrated by a comparison of Tables 3 and 4, thus leave the matrix denuded in these elements.[20] Nevertheless, such features clearly do not have a major impact on the corrosion resistance (especially at 18 °C). It may be that their main effect is to reduce the ability of the material to repassivate once corrosion has initiated at 50 °C, as indicated by the higher maximum currents of fused specimens at this temperature (Fig. 10).

5. Conclusions

- Corrosion of the Ni-Cr-Mo-Si-B coating without vacuum-fusion post-treatment occurs by a series of micropitting and macropitting mechanisms associated with the hard phases and splats, respectively.
- Post-treatment of HVOF-sprayed Ni-Cr-Mo-Si-B coating by polymer impregnation has been shown to have no effect on the corrosion resistance.
- Vacuum-fusion treatment of the as-sprayed coating is beneficial in many aspects such as lowering both the coating and interfacial porosities, increasing the coating density and microhardness, and reducing the microroughness of the as-sprayed surface.
- Vacuum fusion also alters the microstructure and microchemistry of the coating.
- Vacuum-fused coatings corrode by different mechanisms such as matrix corrosion and micropitting than do the as-sprayed or vacuum-fused coatings, but these mechanistic differences do not result in any significant difference in corrosion resistance.

Acknowledgments

This work was made possible by means of an ORS award and a Glasgow University Faculty of Engineering Research Scholarship made to S. Shrestha. The authors also acknowledge Professor J.W. Hancock, Head of the Mechanical Engineering Department, University of Glasgow, and Professor R.L. Reuben, Head of the Mechanical and Chemical Engineering Department, Heriot-Watt University (Edinburgh), for the provision of laboratory facilities.

References

1. H.D. Steffens, M. Gramlich, and K. Nassenstein: *Mater. Sci. Forum*, 1994, vols. 163–165, pp. 559-72.
2. K. Haugen, O. Kvernvold, A. Ronold, and R. Sandberg: *Wear*, 1995, vol. 186, pp. 179-88.
3. F. Ladru, E. Lugscheider, H. Jungklaus, and C. Herbst: *Proc. 1st United Thermal Spray Conf.*, Indianapolis, IN, Sept. 15–18, 1997, ASM International, Materials Park, OH, 1997, pp. 175-81.

4. K. Tani and A. Nakahira: *Proc. 15th Int. Thermal Spray Conf.*, Nice, France, May 25–29, 1998, vol. 2, pp. 1097-2002.
5. G. Barbezat, S. Keller, and G. Wuest: *Proc. 1st United Thermal Spray Conf.*, Indianapolis, IN, Sept. 15–18, 1997, ASM International, Materials Park, OH, 1997, pp. 11-15.
6. J.P. Huchin: *Proc. 15th Int. Thermal Spray Conf.*, Nice, France, May 25–29, 1998, vol. 2, pp. 925-31.
7. A. Neville, T. Hodgkiess, and J.T. Dallas: *Wear*, 1995, vol. 186–187, pp. 497-507.
8. A. Neville and T. Hodgkiess: *Br. Corr. J.*, 1997, vol. 32 (3), pp. 197-205.
9. A. Ashary and R.C. Tucker: *Surface Coatings Technol.*, 1991, vol. 49, pp. 78-82.
10. A. Neville and T. Hodgkiess: *Surface Eng.*, 1996, vol. 12 (4), pp. 303-12.
11. A. Neville and T. Hodgkiess: *Proc. 1st United Thermal Spray Conf.*, Indianapolis, Sept. 15–18, 1997, ASM International, Materials Park, OH, 1997, pp. 161-66.
12. A. Neville and T. Hodgkiess: *Corr. Sci.*, 1996, vol. 38 (6), pp. 927-56.
13. E. Lugscheider, P. Jokiel, V. Messeschmidt, and G. Beckschulte: *Inst. Mater., London*, 1993, pp. 46-51.
14. B. Wielage, U. Hofmann, S. Steinhauser, and G. Zimmermann: *Surface Eng.*, 1998, vol. 14 (2), pp. 136-38.
15. M.C. Garcia-Alonso, M.L. Escudero, V. Lopez, and A Macias: *Iron Steel Inst. Jpn. Int.*, 1997, vol. 37 (2), pp. 161-68.
16. K. Sridhar, A.S. Khanna, and M.B. Deshmukh: *Proc. 15th Int. Thermal Spray Conf.*, Nice, France, May 25–29, 1998, vol. 1, pp. 43-48.
17. S. Shrestha: Ph.D. Thesis, University of Glasgow, Glasgow, United Kingdom, 2000.
18. S. Tobe: *Proc. 15th Int. Thermal Spray Conf.*, Nice, France, May 25–29, 1998, vol. 1, pp. 3-11.
19. M.F. Smith, R.C. Dykhuizen, and R.A. Neiser: *Proc. 1st United Thermal Spray Conf.*, Indianapolis, IN, Sept. 15–18, 1997, ASM International, Materials Park, OH, 1997, pp. 885-93.
20. I. Kretschmer, P. Heimgartner, R. Polak, and P.A. Kammer: *Proc. 1st United Thermal Spray Conf.*, Indianapolis, IN, Sept. 15–18, 1997, ASM International, Materials Park, OH, 1997, pp. 199-202.